

TECHNICAL ARTICLE

Open Access



CFD simulation and validation of self-cleaning on solar panel surfaces with superhydrophilic coating

Jin Hu^{1*}, Nicolas Bodard¹, Osmann Sari¹ and Saffa Riffat²

Abstract

Solar panel conversion efficiency, typically in the twenty percent range, is reduced by dust, grime, pollen, and other particulates that accumulate on the solar panel. Cleaning dirty panels to maintain peak efficiency, which is especially hard to do for large solar-panel arrays. To develop a transparent, anti-soiling Nano-TiO₂ coating to minimize the need for occasional cleaning is the purpose of this study. In our study, a 2D rainwater runoff model along tilted solar panel surface based on the Nusselt solution was established to have better understanding and predicting the behavior of runoff rain water, especially in contact with solar-panel surfaces with Nano-TiO₂ coating. Our simulation results demonstrate that solar-panel surfaces with Nano-TiO₂ coating create a superhydrophilic surface which cannot hold water, showing features of more pronounced in increasing runoff water film velocity comparing to the uncoated surfaces during raining event resulting in better effect of self-cleaning. Validation of our model was performed on titled solar panels for real time outdoor exposure testing in Switzerland. It is found that the dust particles are not easy to adhere to the coated surfaces of the slides comparing with uncoated surfaces, showing great potential for its use in harsh environmental conditions. This study suggests that superhydrophilic self-cleaning solar panel coating maximize energy collection and increases the solar panel's energy efficiency.

Keywords: Nano-TiO₂ coating; Self-cleaning; 2D runoff model; Solar-panel surfaces

Introduction

Solar PV technology is well-proven for producing electricity, where the global production has been increasing 370 times than that in 1992 (Kazmerski 2011). The output of a PV module is usually rated by manufacturers under Standard Test Conditions (STC), where each module is tested under a temperature of 25 °C; solar radiation of 1000 W/m², air mass of 1.5 spectra and wind speed of 2 m/s. However, these conditions are different from the conditions in the practical fields. With the increasing use of PV systems, it is vital to study meteorological parameters that affect the performance of these systems such as humidity, dust, temperature and wind speed.

The effect of dust on PV modules performance has been investigated in different ways as can be found in the literature. Wakim (1981) claimed that 17 % of PV power is lost due to dust deposition on PV modules in Kuwait city. Sayigh *et al.* (1985) reported the effect of

dust accumulation on the tilted glass plates revealed a reduction in plate-transmittance ranging from 64 to 17 %, for tilt angles ranging from 0° to 60° respectively after 38 days of exposure. A reduction of 30 % in useful energy gain was observed by the horizontal collector after three days of dust accumulation. Salim *et al.* (1988) indicated that a 32 % reduction in performance after eight months occurred under desert conditions in KSA. Goossens and Kerschaever (1999) showed that the deposition of fine dust particles on the cover of PV modules significantly affects the performance of these modules. Katz (2008) reported that the dirt on PV modules caused a 2 % of power reduction as compared to clean PV modules. However, Sayigh (2009) reported a power decrease of about 11.5 % in a PV module exposed for only 72 h in Riyadh, Saudi Arabia.

Kazem *et al.* (2013) recently conducted experiments concerning the effects of air pollutants including red soil, ash, sand, calcium carbonate, and silica on the solar power generated. Their results show that the reduction in PV voltage and power strongly depends on pollutant type and deposition level. The highest reduction in PV

* Correspondence: jin.hu@heig-vd.ch

¹Institute of Thermal Engineering (IGT), University of Applied Sciences of Western Switzerland, Av. des Sports 20, CH-1400 Yverdon-les-Bains, Switzerland

Full list of author information is available at the end of the article

voltage (25 %) is recorded when the ash pollutant is used.

A study conducted by Harvard University students showed that energy losses of solar panels due to soiling (of the surface) vary between 9 and 20 % of the possible energy absorption (Wack 1980). This is a significant decrease of energy and brings the subject of solar panel cleaning to attention. However, most solar panels are placed in regions with difficult accessibility such as a roof. This combined with high voltage proximity makes cleaning solar panels expensive and difficult.

There are numerous ways to clean a surface: from abrasive techniques like sandblasting to laser cleaning and water spraying. Some of the factors of conventional methods shall be mentioned: Possible damage caused by aggressive cleaning methods that may roughen the surface and the surface is more susceptible to new smudging in the future; as cleaning is an intensive work, therefore costs a lot for labor work; massive use of chemicals in cleaning will cause environmental problems.

Blossey (2003) claimed two routes to self-cleaning are emerging, which work by the removal of dirt by either film or droplet flow. In other words, water film flows, either on hydrophilic surface or water drop flow on hydrophobic surface, are methods to achieve self-cleaning.

Nano-TiO₂ transparent coating can make a substrate surface to be photocatalytic and hydrophilic. UV-radiation from daylight reacts with dirt and organic deposits, oxidizes them and breaks their adherence to the surface. There is sufficient evidence to support the removal of organic contaminants (Ohtsu *et al.* 2009) and bacteria (Dunnill *et al.* 2009) adsorbed on a TiO₂ surface by the photooxidation process. Due to TiO₂ films that exhibit hydrophilicity (Ohtsu *et al.* 2009), surface raindrops spread as a film on the surface, ensuring the loosened dirt particles are carried away from the surface during rainy weather.

The phenomenon of soiled and stained facades is serious in the cities. Industrial pollution has increased these problems. Especially in densely populated urban areas, building facades are covered by inorganic pollutants like nitrogen oxides and organic pollutants like benzene. All these pollutants are destructive for buildings and unhealthy for people. Nano-TiO₂ coating can be easily applied on facades to reduce the concentration of nitric oxides and other toxic substances like benzene which can provoke respiratory problems and increase smog formation. Hereby, Nano-TiO₂ coating is very good candidate to reduce air pollution in cities.

The purpose of this study is to establish a 2D model of water slide on inclined self-cleaning surface (nano-TiO₂ coated superhydrophilic solid surface) for PVT/solar panels, specifically targeting at solar panel surfaces. The self-cleaning effect of the super-hydrophilic coating is

conducted on PV panels under natural environmental conditions in Switzerland.

Superhydrophilic and hydrophilic surfaces

Rhykerd *et al.* (1991) measured ellipsometrically the thickness of the adsorbed water film on a fused silica surface and found it ranging from 2.4 to 9.0 nm, depending on the water vapor pressure. Staszczuk (1985) used gas chromatography to determine the water adsorption isotherm on quartz at 20 °C and found that about sixteen statistical water layers adsorbed from a gas phase saturated with water vapor. Also, similar experiments Janczuk *et al.* (1983) using the chromatographic technique showed that about fifteen statistical water layers may adsorb onto a marble surface. Water films with thicknesses from 1.0 to 8.0 nm were also reported for muscovite mica (Perevertaev *et al.* 1979).

Anna Lee *et al.* (2012) studied the condensation behaviors of the surfaces with different wettability and roughness. They concluded that the hydrophilic surfaces are superior in condensation rate from its early stage when the dry surfaces directly face humid air. In their experiments, where the film thickness δ on hydrophilic surface is estimated by the Nusselt theory that balances the viscous shear force and the gravitational force (Incropera and DeWitt 2002)

$$\delta \approx \left[\frac{4k_l \mu_l (T_s - T_w) L_p}{g \rho (\rho - \rho_a) h_{fg}} \right]^{\frac{1}{4}} \quad (1)$$

They obtained δ is $\sim 85 \mu\text{m}$.

It is commonly accepted that in the vicinity of hydrophilic interfaces water organizes into ice-like water, which project from the surface by a few nanometers (Noguchi *et al.* 2008; Tian *et al.* 2008; Smith *et al.* 2004). Yoo *et al.* (2011) used NMR spectroscopy to study impact of hydrophilic surfaces on interfacial water dynamics. Their findings confirm the existence of highly restricted water layers adsorbed onto hydrophilic surfaces and dynamically stable water beyond the first hydration layers. Thus, aqueous regions on the order of micrometers are dynamically different from bulk water.

Precursor film

When a perfectly wetting liquid spreads relatively slowly on a clean smooth substrate, a very thin precursor film may propagate ahead of the apparent or macroscopic wetting line with the average thickness of the film determined by material property of liquid phase and solid wall (Heslot *et al.* 1989 and 1990). The first reported observation of an 'invisible' film spreading ahead of the edge of a macroscopic drop stems from the pioneering work by (Hardy 1919 and 1936), Hardy was unable to detect its presence

directly at that time. Numerous studies have subsequently confirmed the existence of precursor films using ellipsometry Beaglehole (1989); Bascom *et al.* (1964), interference microscopy patterns Bascom *et al.* (1964), and polarized reflection microscopy (Ausserre *et al.* 1986). Simultaneous observations of the moving droplet and of the fringe pattern by the laser ellipsometry (Ueno and Watanabe 2005) reveal the existence of the precursor film, which is ahead the moving contact line and traveled with varying its profile.

If the fluid is perfectly wetting, we have seen that van der Waals forces lead to the formation of a precursor film in front of the contact line (de Gennes 1985). Wang (2003) in his thesis claimed the surface feature, particularly micro-structure or roughness, promotes the formation and development of thin precursor film, they claimed that the precursor film spreads much faster than the movement of the apparent contact line (ACL) on a rough solid surface. Amit Sah (2014) studied precursor film with glass capillaries and cover slips. His experimental results imply that the precursor film moving ahead of the contact line controls the wetting behavior. Yuan and Zhao (2010) using molecular dynamics (MD) simulations to explore the atomic details and the transport properties of the precursor film in dynamic wetting. Their results showed that the molecules which finally formed the precursor film came almost from the surface in the initial state of the droplet. The fast propagation of the precursor film is owing to continuous and very fast diffusing of the surface water molecules that have the highest self-diffusion coefficient to the front of the precursor film allows for fast propagation of the precursor film. Precursor film propagates fast with low energy dissipation.

The typical thickness of the precursor film moving in front of macroscopic body of fluid is in the range of 500–3000 Å (Bascom *et al.* 1964; Beaglehole 1989). For a fixed volume of water droplet, according to Tanner's laws (Tanner 1979), the spreading of the macroscopic part of the droplet is rather slow; it would take a very long time

to completely spread a macroscopic drop (Voinov 1976; Tanner 1979). The precursor which advances at a seemingly faster rate than the normal contact line is indeed well documented. It has been found that the velocity at which the precursor film advances depends on the materials of the gas/liquid/solid system and can vary in wide range. Bascom *et al.* 1964 reported the speed of propagation of the precursor film of squalane on stainless steel is about 10^{-4} cm/s while indirect measurement for water on glass Marmur & Leilah (1980) suggest that there the precursor film velocity is of the order of 10 cm/s. As a result, the existence of precursor film makes the ACL moving on the film rather than on a real solid surface. In other words, the ACL moves over the “wet” solid surface instead of the “dry” solid surface.

Precursor film on dry surface

As stated by de Gennes (1985) and Joanny and de Gennes (1984), long-range forces, for example, van der Waals forces, should be taken into account in the spreading phenomenon of precursor film. It is found that, at sufficiently short time, when the macroscopic droplet still acts as a reservoir, the behavior of the precursor film is diffusive and the radial extension length (l) on a macroscopic scale follows a universal time dependence (t) of the form:

$$l^2 = Dt \quad (2)$$

where D is the diffusion coefficient of the liquid within the precursor film. It is different from the conventional diffusion coefficient describing the random motion of particles in the bulk liquid phase or on solid substrates. As a matter of fact, D also depends on the driving forces which cause the film spreading.

As shown in Fig. 1, the macroscopic wedge of liquid is advancing at a constant velocity U on a solid dry surface into an external air. The dynamic contact angle is θ_D and the wedge is preceded by a precursor film of length l . The dynamic contact angle θ_D , which depends on the

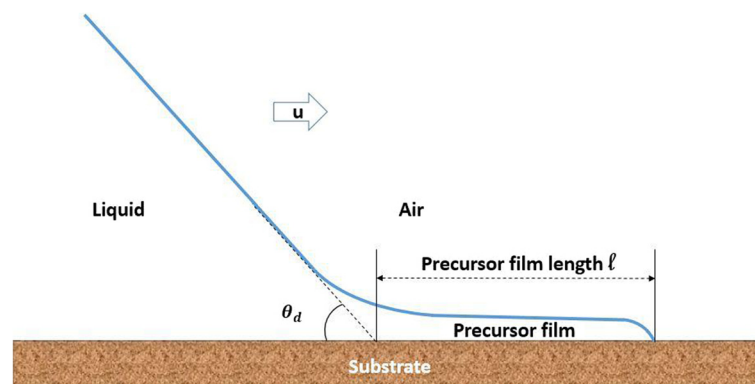


Fig. 1 Precursor film on dry surface

advancing velocity U , the liquid/vapor interfacial tension γ and the liquid viscosity η through Tanner's law (Tanner 1979).

Precursor film on superhydrophilic/hydrophilic surface

Hydrophilic surfaces adsorb water from the environment and the amount of water depositing on the hydrophilic surface depends on the relative humidity. It is generally accepted that under ordinary atmospheric conditions, hydrophilic surfaces adsorb at least a monolayer of water. For example, a clean glass surface is covered with a monolayer of adsorbed water at relative humidity of around 30–50 % at 20 °C (Razouk and Salem 1948). Formation of a water film composed of as many as twenty molecular layers, or more, may occur at the clean surface of high-energy solids, especially at high relative humidities >90–95 % (Zisman 1965).

Water appears to have unusual lubricating properties and usually gives wearless friction with no stick slip (Raviv et al. 2004). It is also interesting that a 0.25 nm thick water film between two mica surfaces is sufficient to bring the coefficient of friction down to 0.01–0.02, a value that corresponds to the unusually low friction of ice. The effectiveness of water film only 0.25 nm thick to lower the friction force by more than an order of magnitude is attributed to the "hydrophilicity" of the mica surface and to the existence of a strongly repulsive short-range hydration force between such surfaces in aqueous solutions, which effectively removes the adhesion-controlled contribution to the friction force (Berman et al. 1998). Clearly, a single monolayer of water can be a very good lubricant - much better than most other monomolecular liquid films (Ruths & Israelachvili 2011). It also stresses the inertial nature of the spreading: a viscopillary motion would have been much quicker on a pre-wetted substrate, because of the lubricating effect of this water layer (Biance et al. 2004).

Villette et al. (1996) focused specifically on the role of water on the spreading of molecular films of non-volatile liquids PDMS, PDMS with hydroxyl ends (PDMS-OH)

and TK on oxidized silicon wafers. Their analysis revealed the dependence of D on relative humidity (RH). Overall, within the range of 20–90 % RH, D varies by more than two orders of magnitude, attaining the values observed for mesoscopic precursor films. This agrees well with the observations made by (Valignat et al. 1998 and Vou'e et al. 1999). Such a remarkable enhancement of D has been explained by the fact that at this value of RH the patches of water on the substrate start to overlap and form a tortuous connected structure on which the spreading of molecules encounters a very low friction. This implies on superhydrophilic/hydrophilic surface, the length of precursor film is much longer than that of the ordinary surfaces. When viewed at the atomic scale, the precursor film plays an important role in the dynamic wetting process on hydrophilic substrate.

As shown in Fig. 2, before the spreading of liquid on superhydrophilic/hydrophilic surface, the solid surface is already covered with a thin film of water with thickness h due to absorption/condensation on hydrophilic surface. The advancing velocity of the macroscopic wedge of liquid is not the average velocity u , but rather u' (Joanny and de Gennes 1984). Obviously, if $h \neq 0$, $u' > u$.

$$u' = \frac{\xi}{\xi - h} u \quad (3)$$

We conclude when the superhydrophilic/hydrophilic was previously wetted by a very thin layer of the inner water, the advancing velocity of the macroscopic wedge of liquid is faster than that of dry solid surface.

Water spreading dynamics

When a liquid drop contacts a wettable surface, the liquid spreads over the solid to minimize the total surface energy. For low viscous liquids (as water), a power law of the drop spreading can be observed during almost all the evolution varying the relative different contributions (inertia, gravity, viscosity, density, volume, surface tension...etc.).

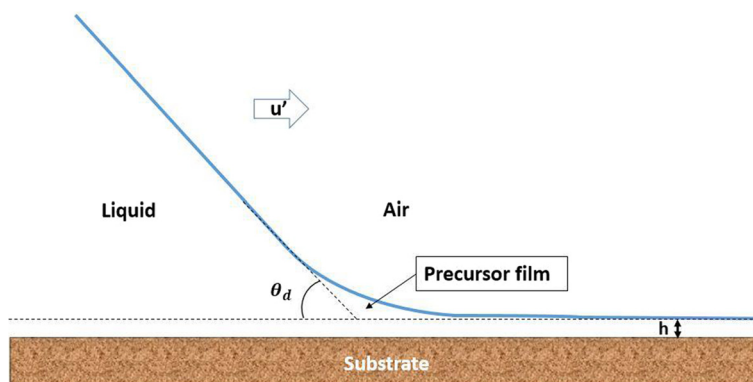


Fig. 2 Precursor film on superhydrophilic/hydrophilic surface

Dynamic wetting may proceed with three stages. About 1 to 100 μs after the drop contacts the surface, inertia of the moving drop resists the capillary force that drives a high speed spreading (in the order of 1 m/s). The spreading dynamics of low-viscosity drops (e.g. water) follow a power law $r = Kt^{0.5}$, which is independent of the liquid viscosity and surface wettability (Biance *et al.* 2004; Bird *et al.* 2008; Carlson *et al.* 2011; Chen *et al.* 2011; Winkels *et al.* 2012; Stapelbroek *et al.* 2014). The quantity r is the spreading radius, t is the spreading time and K is a coefficient.

With time between ~ 0.1 to 10 ms, the drop spreading speed is still high (~ 0.1 m/s), wetting is still dominated by inertia. However, the surface wettability starts to influence spreading and the spreading radius grows with time according to another power law $r = K' t^\alpha$ (Bird *et al.* 2008). K' is another coefficient and the exponent α is only dependent on the equilibrium contact angle θ_{eq} . Experiments of Stapelbroek *et al.* (2014) reveal a deviation from a pure power-law, the cross-over from the 1/2 power law to the final equilibrium radius displays a universal dynamics. This cross-over is governed only by the final contact angle, regardless of the details of the substrate.

Bird *et al.* (2008) considered the energy dissipation during spreading and derived a power law which associates α with θ_{eq} .

$$\alpha = C \sqrt{F(\theta_{eq}) + \cos\theta_{eq}} \quad (4)$$

Experimental study showed that α increases from ~ 0.25 for $\theta_{eq} \approx 120^\circ$ to ~ 0.5 for $\theta_{eq} \approx 0^\circ$ (Bird *et al.* 2008).

After the two inertial stages aforementioned, on strongly hydrophilic ($\theta_{eq} < \sim 57.3^\circ$ or 1 radian) or completely wetting surfaces ($\theta_{eq} \approx 0^\circ$), a third wetting stage was found. In this stage, the wetting speed is much slower than in the previous two stages, it takes a much longer time for viscous liquids to completely spread and $R_e < 1$. In this long time limit stage, the viscous friction inside the drop is the main source opposing capillarity. The wetting dynamics follows 1/10 power law for small drops of negligible gravity effects (Tanner 1979; Cazabat and Cohen-Stuart 1986; Levinson *et al.* 1988; Chen and Wada 1989; Rafai *et al.* 2002):

$$r = R_0 \left(\frac{r}{\mu R_0} \right)^{0.1} t^{0.1} \quad (5)$$

For large drops dominating by gravity effects, the radius of spreading pattern is to follow Lopez's law of a 1/8 power law in the gravitational regime for large droplets (Smith; Lopez *et al.* 1976; Yeo 2008). However, as the radius grows beyond the capillary length, the drop changes toward a "pancake" shape of constant thickness, curved only at the rim, and the main driving force is now gravity, leading

to $n = 1/7$ (Kavehpour *et al.* 2002; Oron *et al.* 1997; Ehrhard 1993).

This extremely slow dynamics emerges from a balance between surface tension and viscous forces close to the contact line (Bonn *et al.* 2009).

Runoff equations for thin film flow

The model of gravity-driven flow was based on the assumption that the inclined solid surface is initially covered with a liquid film. We focus on the gravity-driven film flow. The solid surface is often initially dry and is gradually covered by the liquid film as the leading edge of the film moves down under the action of gravity.

Consider a film of viscous liquid of density ρ and viscosity μ , flowing down a plane inclined at an angle α , as illustrated in Fig. 3, and the flow is assumed to be two-dimensional, with no variations in the direction normal to the plane of the sketch. Far away from the leading edge the film is approximately flat and, therefore, the flow is described by the constant-thickness solution, with the average flow velocity $\rho g d^2 \sin(\alpha/3\mu)$. It is convenient to define the characteristic flow velocity by:

$$U = \frac{\rho g d^2}{\mu} \sin\alpha \quad (6)$$

Here, the surface tension σ is assumed constant. At the leading edge of the film, the liquid-gas interface is assumed to be meeting the solid surface at a contact angle θ , as shown in Fig. 3 and the capillary number based on this velocity as:

$$Ca = \frac{\mu U}{\sigma} \quad (7)$$

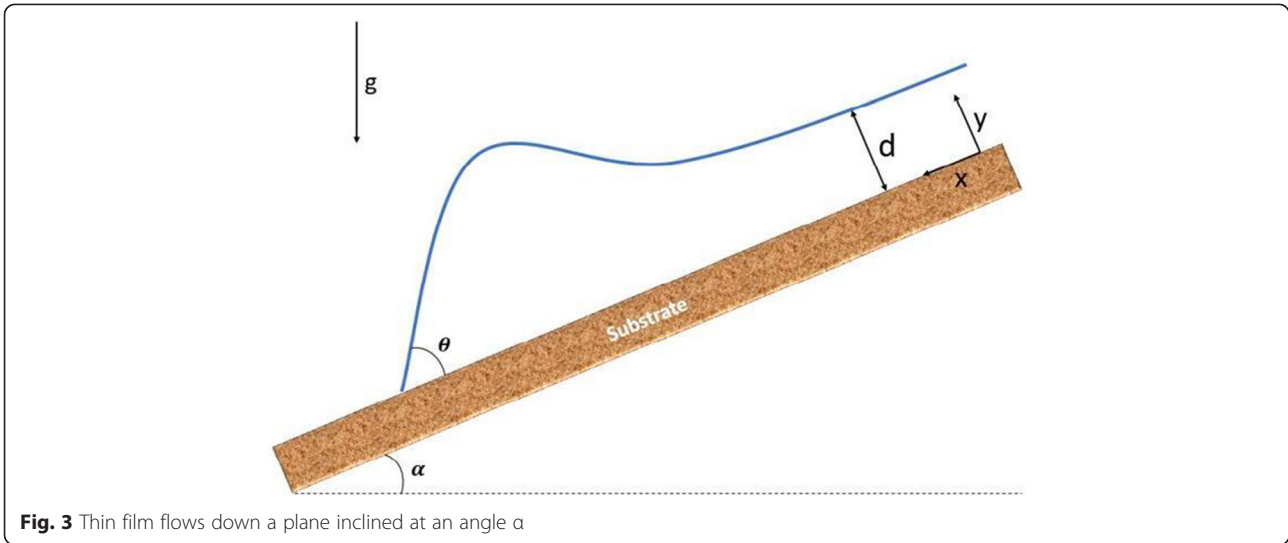
Lubrication approximation of thin liquid film

We model the spreading of a thin liquid film on an inclined substrate. We use the lubrication approximation of the Navier-Stokes equations, and we provide appropriate initial and boundary conditions. Within the framework of the lubrication approximation, the velocity of the fluid is depth-averaged over the thickness of the film (Greenspan 1978). Following this approach, one obtains the average fluid velocity,

$$\mathbf{v} = (u, v) \quad (8)$$

$$\mathbf{v} = -\frac{h^2}{3\mu} [\nabla p - \rho g \sin\alpha \mathbf{i}] \quad (9)$$

where $\nabla = (\partial x, \partial y)$, h is the fluid thickness, p is the pressure, μ is the viscosity, ρ is the density, g is gravity, and α is the inclination angle of the plane of the substrate. The coordinate frame is chosen so that \mathbf{i} points down the incline, and \mathbf{j} is the transverse direction in the plane. We note that Eq. 10



assumes no-slip boundary condition at the fluid/solid interface. The pressure includes the hydrostatic component, and the contribution following from the Laplace-Young boundary condition at the fluid-air interface.

$$p = -\gamma \nabla^2 h + \rho g h \cos \alpha \tag{10}$$

Nondimensionalization of thin film equations

We consider a layer of liquid on a plane substrate inclined to the horizontal at an angle α . The fluid is Newtonian and incompressible of density ρ , viscosity μ and surface tension γ . We start with the following 2-D lubrication equation (Diez and Kondic 2002):

$$\begin{aligned} \frac{\partial h}{\partial t} &= -\nabla \cdot (h \mathbf{v}) \\ &= -\frac{1}{3\mu} \nabla [y h^3 \nabla^2 \nabla^2 h - \rho g h^3 \nabla h \cos \alpha + \rho g h \sin \alpha \mathbf{i}] \end{aligned} \tag{11}$$

Here h is the height of the fluid given as a function of x and y . The (x, y) plane is parallel to the substrate and the x direction is the direction of the slope. Then, g is the acceleration of gravity and \mathbf{i} is the unit vector in the x direction. There are several possibilities to obtain non-dimensional variables.

All the theoretical and computational methods of the spreading drop problem require some regularizing mechanism - either assumption of a precursor film in front of the apparent contact line (Troian *et al.* 1989; Bertozzi and Brenner 1997), or relaxing the no-slip boundary condition at fluid–solid interface (Greenspan 1978; Hocking and Rivers 1982). However, the computational performance of the precursor film model is shown to be much better than that of various slip models. For this reason, in this work, we also use a precursor film model, which assumes that

the solid surface is pre-wetted with the wetting layer thickness h' (scaled by h) as a regularizing method in this work.

Thus, the lubrication approximation reduces the Navier–Stokes equations to this nonlinear fourth order partial differential equations that govern the time evolution of the film thickness $h(x, y, t)$.

As we focus on long-scale evolution of liquid films, we scale h by the height h' of the precursor film and we define the scaled in-plane coordinates and time by $(x^*, y^*, t^*) = \left(\frac{x}{x_c}, \frac{y}{y_c}, \frac{t}{t_c}\right)$ where

$$x_c = \left(\frac{a^2 h'}{\sin \alpha}\right)^{\frac{1}{3}} \tag{12}$$

$$t_c = \frac{3\mu}{\gamma} \frac{a^2 x_c}{h'^2 \sin \alpha} \tag{13}$$

And $a = \sqrt{\frac{\gamma}{\rho g}}$ is the capillary length, the velocity scale is chosen naturally as $U = \frac{x_c}{t_c}$, and the capillary number is defined by $Ca = \frac{\mu U}{\gamma}$. Using this dimensionless form, Eq. (12) for $h^* = \frac{h}{h'}$, the lubrication equation given above becomes:

$$\frac{\partial h^*}{\partial t^*} + \frac{\partial}{\partial x^*} \left\{ h^{*3} \left(\frac{\partial^3 h^*}{\partial x^{*3}} - D(\alpha) \frac{\partial h^*}{\partial x^*} + 1 \right) \right\} = 0 \tag{14}$$

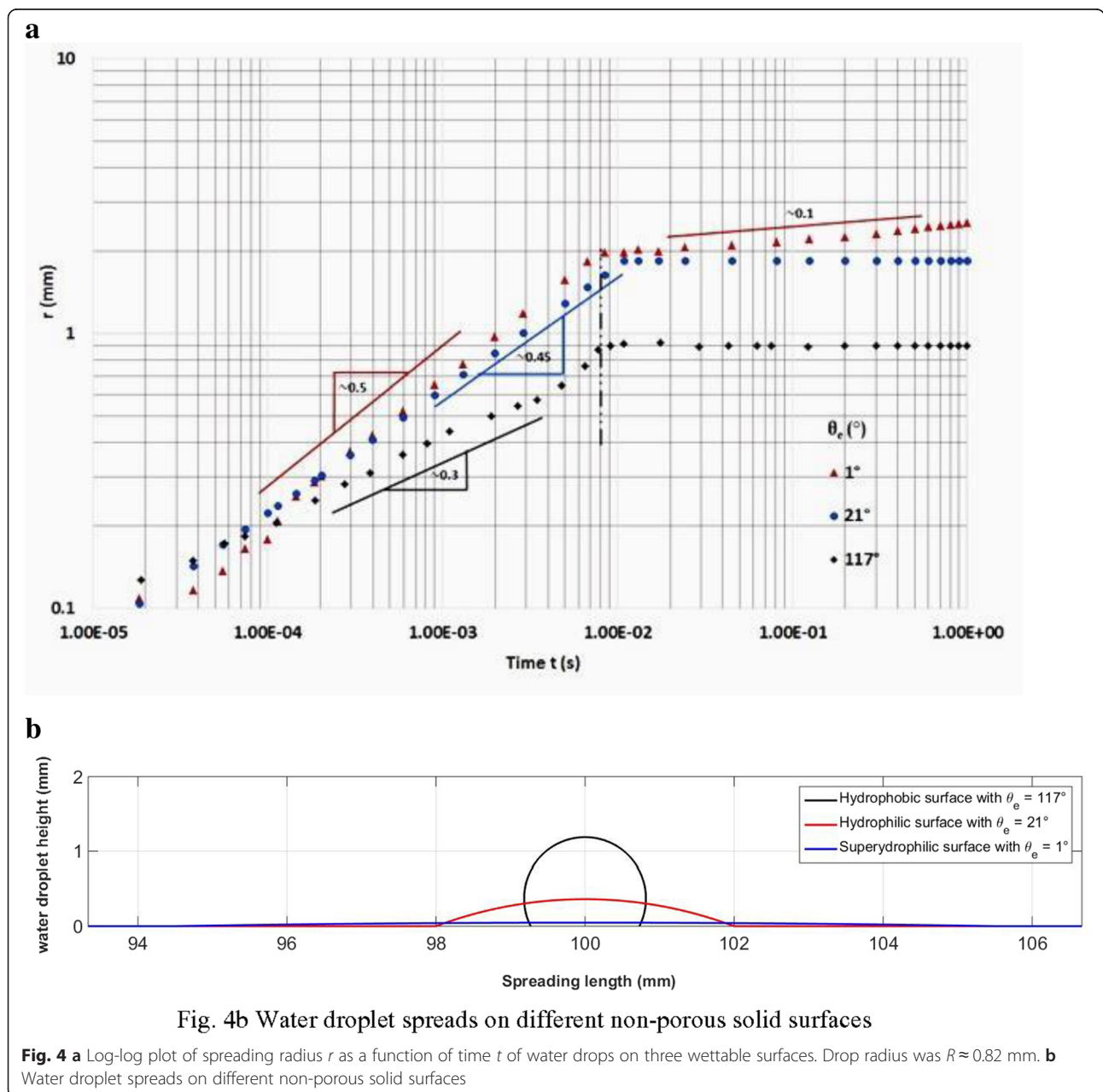
where the single dimensionless parameter $D(\alpha) = (3Ca)^{\frac{1}{3}} \cot(\alpha)$ measures the influence of gravity. We note that the lubrication approximation requires the slope of the free surface to be small.

Simulation results and discussion

Simulation of water droplet spreading on non-porous flat solid surface

We consider a spherical droplet of volume $V = \frac{4}{3}\pi r^3$ deposited on a horizontal wall that enters in contact with a horizontal wettable surface at time $t = 0$. The initial water droplet radius chosen for this simulation is $R = 0.82$ mm. Water surface tension is $\sigma = 0.0727$ Nm^{-1} ; the density of water is equal to $\rho = 1000$ kg/m^3 . To identify the effects of surface wettability, surfaces with equilibrium contact angles from $\sim 0^\circ$ to $\sim 117^\circ$ were studied.

We chose $\theta_e = 1^\circ$ as a superhydrophilic surface (e.g. existing thin water layer, completely wetting); $\theta_e = 21^\circ$ as hydrophilic surface (e.g. n-Octyltriethoxysilane surface, partial wetting); $\theta_e = 117^\circ$ as hydrophobic surface (e.g. triethoxysilane surface). Based on experimental data of Bird et al. (2008), for $0.1 \leq t \leq 8$ ms, we derived the power-law exponent α is about 0.52 and the coefficient C is 1.46 for superhydrophilic surface; for hydrophilic surface, α is about 0.45, the coefficient C is equal to 1.21; for hydrophobic surface, α is about 0.3, the coefficient C is equal to 0.69. By applying Eqs. 15, 16 and 17, we obtained the simulation results as shown in Fig. 4a and b



$$\frac{r}{R} = C \left(\frac{t}{\tau} \right)^\alpha \tag{15}$$

$$\tau = \sqrt{\frac{\rho R^3}{\gamma}} \tag{16}$$

$$r = C \left(\frac{\gamma t}{\rho} \right)^\alpha R^{1-\frac{3\alpha}{2}} \tag{17}$$

Figure 4a shows the log-log plot of time t vs spreading radius r of water drops spreading on three surfaces with different wettability. When time is $t < 0.1$ ms, the wetting follows a power law

$r = K t^{0.5}$. For $0.1 \leq t \leq 8$ ms, the wetting followed a power law $r = K' t^\alpha$. The slope, i.e. α is dependent on the surface wettability and increases from ~ 0.3 to ~ 0.5 while θ_{eq} decreases from $\sim 117^\circ$ to $\sim 0^\circ$, which was consistent with previous studies (Bird *et al.* 2008). Fig. 4a clearly reveals that the wetting condition has now significant effect on the spreading rate. As the equilibrium contact angle increases, demonstrates a monotonic decrease in the power-law exponent. Drops spread faster on relatively hydrophilic surfaces than on relatively hydrophobic surfaces. At the same time, wetted area on relatively hydrophilic surfaces is larger than that on relatively hydrophobic surfaces.

On partially wettable surfaces (here $\theta_e = 21^\circ$) and hydrophobic surface ($\theta_e = 117^\circ$), water drops reached equilibrium after the inertial wetting stage, as shown in Fig. 4a and b. In contrast, on completely wetting surfaces, a slower wetting process was observed for $t \geq 8$ s. The power law fitting of the data gave a slope of ~ 0.1 , which indicates

that spreading was dominated by viscous dissipation (Tanner 1979; Cazabat and Cohen-Stuart 1986).

Simulation of water droplet sliding on non-porous inclined flat solid surface

Hydrophilic surfaces are superior in condensation rate from its early stage whereas dry surfaces directly face humid air (Anna Lee *et al.* 2012). In this study, we use pre-wetted superhydrophilic surfaces caused by condensation as initial boundary conditions.

A single water droplet sliding on non-porous inclined and smooth solid surface (e.g. glass surface) was simulated under three different surface conditions represented by different levels of condensation. They are dry glass surface (thin water film thickness = $0 \mu\text{m}$) and two pre-wetted nano-TiO₂ superhydrophilic surfaces with condensed 50 and $80 \mu\text{m}$ thickness thin water film, respectively. To simplify the simulation, only the top part of the glass is chosen. The length of glass is chosen to be 5 cm. The origin of the X-axis ($x = 0$) is set at the top of the glass. The initial height of the water droplet H_0 is 1.5 mm as shown in Fig. 5a. Simulations of three cases start with the same initial water droplet profile. Simulation results are shown in Fig. 5b. Figure 5b clearly shows that the velocity of the water droplets on superhydrophilic surface is faster than on uncoated glass surface at the same inclined angle. The velocity of water droplet is faster on a superhydrophilic surface with a higher condensation rate.

Simulation of water runoff on non-porous inclined flat solid surface

A water runoff on non-porous inclined smooth glass was simulated under three different surface conditions

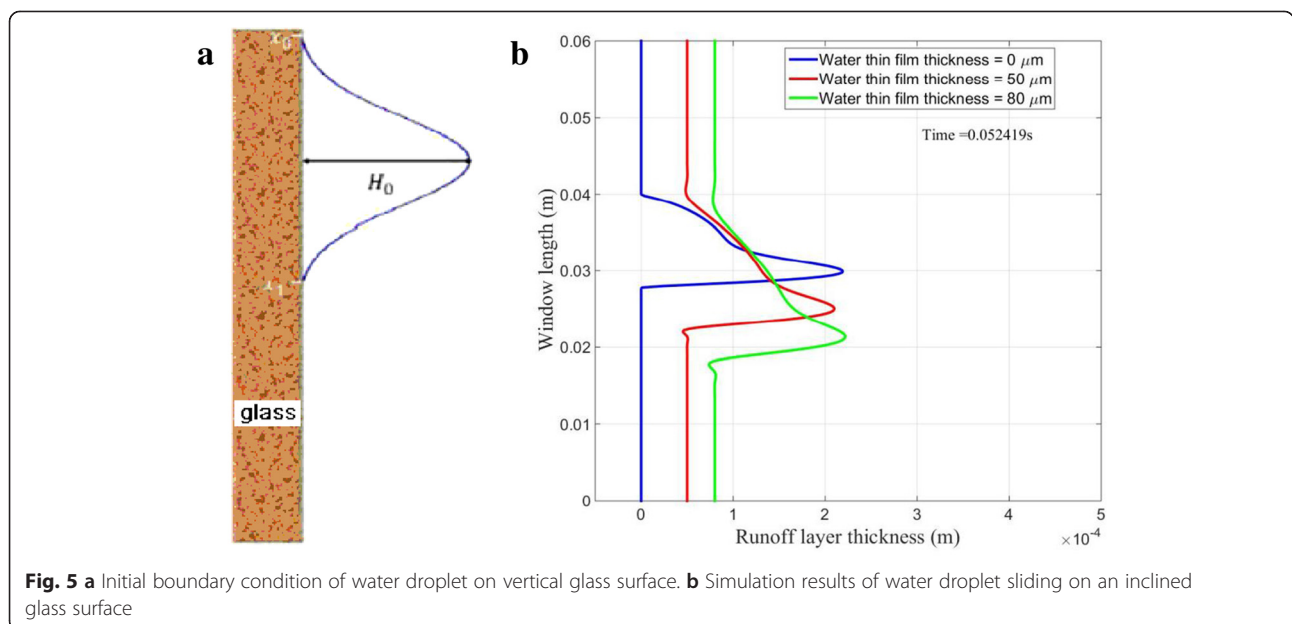


Fig. 5 a Initial boundary condition of water droplet on vertical glass surface. **b** Simulation results of water droplet sliding on an inclined glass surface

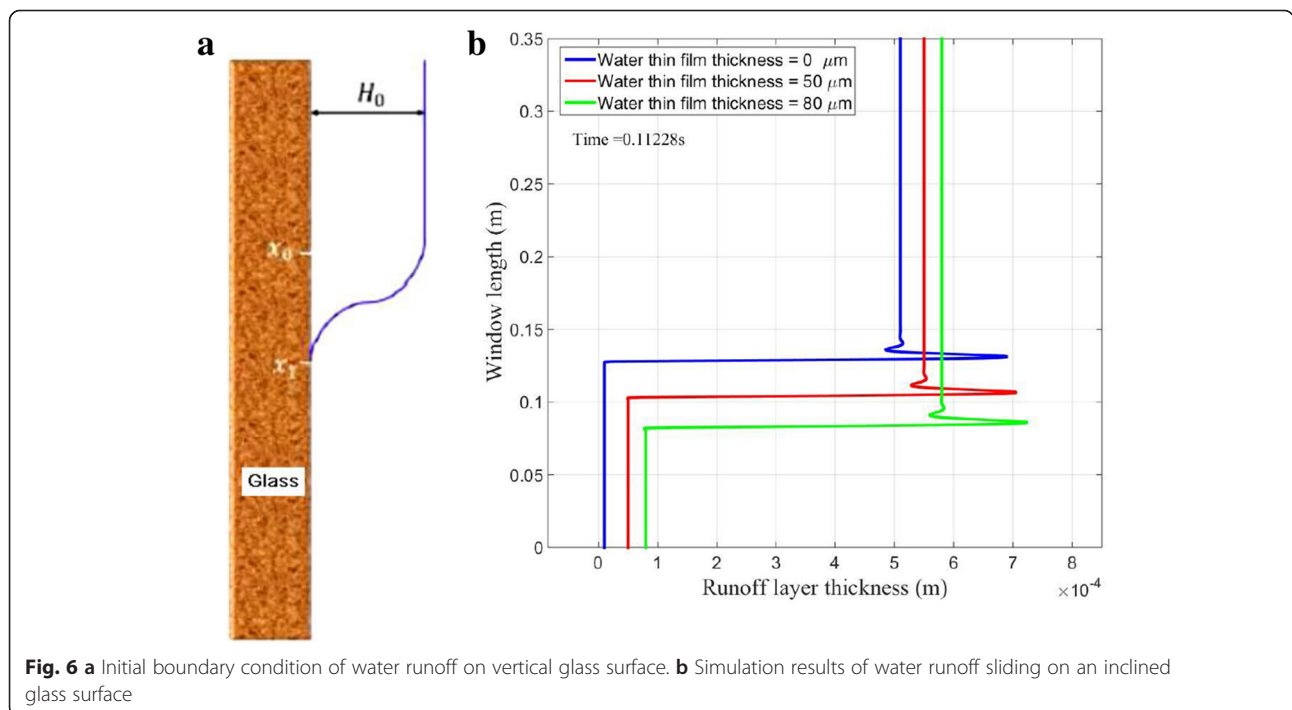
represented by different levels of condensation aforementioned. The origin of the x -axis ($x = 0$) is set on the top of the glass, with $x_0 = 5$ mm and $x_l = 6$ mm. The initial water runoff thickness H_0 is equal to 0.25 mm. Before x_0 , the water front of the runoff is assumed to have the same thickness as H_0 , which can be expressed as a Neumann boundary condition. The length of the glass is assumed to be 25 cm long. Water runoff from the top of the glass is as shown in Fig. 6a. Figure 6b shows the velocity of the water film on superhydrophilic surface was faster than that of an ordinary surface at the same inclined angle. The velocity of the water film is faster on a superhydrophilic surface with a higher condensation rate.

Effect of fluid flow velocity on the detachment of the adherent particles

Aerosol particles cover a size range from 1 nm to 100 μm in diameter. Particles in the range 0.01 to 10 μm are most stable in suspension. Particles smaller than 0.01 μm in diameter are not stable in the atmosphere; they will either react with oxygen or tend to coagulate into larger units, while those larger than 10 μm readily settle out in air. Most particles with dimensions greater than 10 μm require strong air currents to keep them aloft (Sharma 1994). Smaller particles < 1 μm float in the air for days or weeks, during this time, they can be transported over 1000 km before they deposit. While larger particles sediment quite soon and easily onto environmental surfaces which can become contaminated because of their weight (Dagsson-Waldhauserova et al. 2014).

Particles begin to move on the adhered surface when the combined lift and drag forces produced by the fluid flow field applied to particles become large enough to counteract the attractive forces (e.g. the gravity, Van der Waals force) between the particle and the surface that hold the particle in place. In the study of particles, in linear shear flow, Zoetewij et al. (2009) claimed that the particles are in the boundary layer of the fluid flow; these particles will experience a lift force and a drag force exerted on the particle's body. Both forces are a function of fluid velocity at the position of the particle body. At a certain flow velocity, the particles start to detach from a plate. Among the different possible particle motions (lift, sliding and rotation), particle rotation turns out to be the responsible mechanism of particle removal. Rotation is related to the moment of surface stresses which is also a function of fluid velocity. Dagaonkar (2012) drew a quite similar conclusion, namely that the lift force is strongly a function of the flow velocity of the fluid. Specifically, at high fluid flow velocities, the contribution of the lift force is expected to be higher resulting in the detachment of the larger sized particles.

Grease, dirt particles and other staining materials are easily attached to a surface of a solar panel. In the 'photocatalytic' process of TiO_2 coating, the coating reacts with ultraviolet light to break down the organic dirt on the glass and to reduce the adherence of inorganic dirt. In an earlier study, performed by Chabas et al. (2007), on the behaviors of self-cleaning glass in an urban atmosphere, self-cleaning glass is found to have an evident self-cleaning effect, even



when it is not subjected to water. The field study shows that particulate organic matter (POM) was destroyed by a percentage of 44–48 % on the self-cleaning surface.

Therefore, we deduce higher water film spreading velocity on superhydrophilic surface ought to have larger detachment force on particles and a better effect on washing away loose particles.

Experimental setup

The flow of the liquid film is essential for self-cleaning. To clean a surface, liquid has to transport along the impurities and finally run off the surface. It is the flowing liquid film that carries away the impurities. The purpose of this experiment is to validate our model and to test the effect of self-cleaning coating.

Four identical solar monocrystalline panels as shown in Fig. 7 (Type STP005B-12/DEA) are used for application of self-cleaning testing. They are all placed vertically on the test rig and are exposed to sunshine on the roof; all of them are facing south as shown in Fig. 7. To make comparisons, two solar panels on the right-hand side are coated with Nano-TiO₂ (provided by ZIXILAI Co.LtD) coating, marked with number 1 and 2 respectively; while on the left-hand side, two panels are uncoated, marked with number 3 and 4.

Every 20 min, a connected data acquisition system was obtaining the following data series for 30 s: date and time; global irradiation intensity (W/m²); diffuse irradiation intensity (W/m²); voltage (V); current (A); surface temperature (°C). After temperature compensation, voltage *U* and current *I* will be used for analyzing output power.

At first four identical solar panels were cleaned thoroughly by water and then dried in air. Furthermore, we exposed them to air for four days. Their performance was measured to detect differences in power generation as a pre-coating test for a comparison of these four

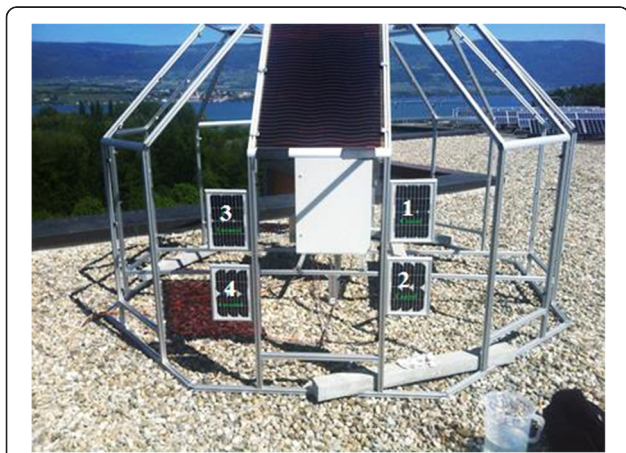


Fig. 7 Solar monocrystalline panels test rig for self-cleaning tests

panels. Afterwards, they were thoroughly cleaned again to remove all dust/contaminates on the surfaces. Two solar panels on the right-hand side of Fig. 7 were coated with nano-TiO₂ coating and other two panels on the left-hand side of Fig. 7 were uncoated. Then they were exposed in air for one day, to perform a post-coating test to detect if the nano-TiO₂ coating affects solar cell performance. Photocatalysis is more efficient, because TiO₂ particles are finely divided and highly dispersed (as shown in Fig. 8a) in order to give the highest surface contact with the surrounding environment. Due to strong wind on the roof and relatively good air quality in the test region, hardly any contamination was detected on some other test solar panels, which are undergoing out-door exposure for one year. To simulate the effects of heavily polluted rainwater, applied to solar cells in a real situation, a “muddy water” mixture consisting of 1.5 g wood ash, representing an ash pollutant, due to the ash pollutant caused the highest reduction in PV voltage (25 %). This was recorded by Kazem et al. (2013). In this work, 500 ml water was sprayed onto the surfaces of these four panels numerous times until they dried (this is shown in Fig. 8b and c). Afterwards, their performance was measured in the following days as extremity tests.

Experimental results

Reflection and light transmittance of Nano-TiO₂ coating

We recently conducted the spectrometric analysis of Nano-TiO₂ coating on PV panels. As we may notice in Fig. 9, in the wave length between 400 to 1200 nm, the reflection on coated surface seems to be 2 ~ 3 % less than that of uncoated surface. Reflections on solar panels need to be avoided. Less reflective surface can be important in increasing a module's output power. In contrast to light reflection, in the same range of wave length, coated PVT panels shows 2 ~ 3 % more light transmittance than that of uncoated PVT panels. High light transmittance means more photons are absorbed by the solar cells, and more power is generated. We conclude that Nano-TiO₂ coating itself has no side effect on the solar cell performance whatsoever. This was very significant since the solar cells could then be coated to improve its other properties without damaging the initial raw performance. Applying this Nano-TiO₂ coating on the surface of a clean PV module will potentially increase the efficiency comparing with other coatings which most likely reduce the transmissivity of sunlight.

The output energy of solar panels

The output of a solar panel is usually stated in Watt, and the Watt (the amount of electric power) is determined by multiplying the rated voltage *V* by the rated amperage *I*. Both voltage and current were adjusted with the temperature compensation. As our data acquisition

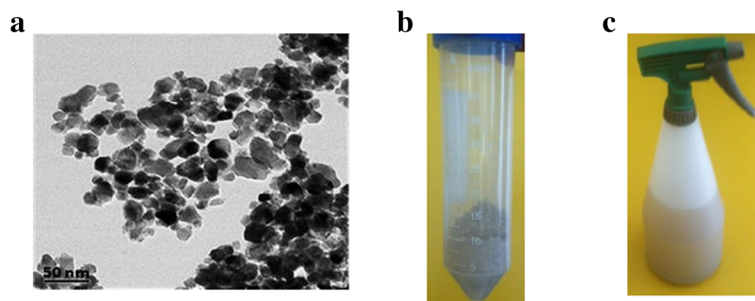


Fig. 8 a Nano-sized particles of TiO₂ (photo provided by ZIXILAI Co.Ltd). b Wood ashes. c Muddy water

system obtains data continuously for thirty seconds every twenty minutes, we use the mean value of I and V within these 30s to obtain the power. By integrating the output power over the testing period, we obtain the curve of “Integrated energy output of testing solar panels via time”. As it can be seen from Fig. 10, a high peak on the figure means a higher energy gain (the weather was sunny, warm and dry), while a low peak is related to a low energy gain (the weather was rainy/cloudy and with a relatively high humidity).

Out-door self-cleaning performance comparison

Figure 11a shows in a pre-coating test, that panels to be coated have a slightly better performance (~2.6 % more energy) than uncoated panels. In a post-coating test, as shown in Fig. 11b, coated panels generated ~6.2 % more energy than uncoated panels (net increase ~3.6 %). This is due to coated surfaces that show less light reflection and smaller transmittance than uncoated surfaces resulting in more generated power.

In an extremity test, solid particles from evaporated muddy water were located on the panel surface. They degraded PV performance very much. However, coated panels generate ~8 % more energy than uncoated panels. This is shown in Fig. 11c (net increase ~5.4 %).

Thanks to two major merits of TiO₂ coating, when a compound (either an organic soil or a pollutant) is present on the surface of nano-TiO₂ coating, it can be degraded by redox reactions involving highly reactive transient species in the presence of UV light. Then, the degradation products are either stored in the coating or washed off the surface by rain water. In addition, Nano-TiO₂ coating is also super-hydrophilic and has high water spreading speed; the super hydrophilicity prevents the formation of water droplets. Water molecules will spread flat immediately to form a thin and uniform water film. This means once there is rain, the rain water forms a uniform film on the coated solar panel surface, which accelerates runoff water spreading and flow, that removes soiling and deters the formation of drying marks as well, and finally results in a better energy generation.

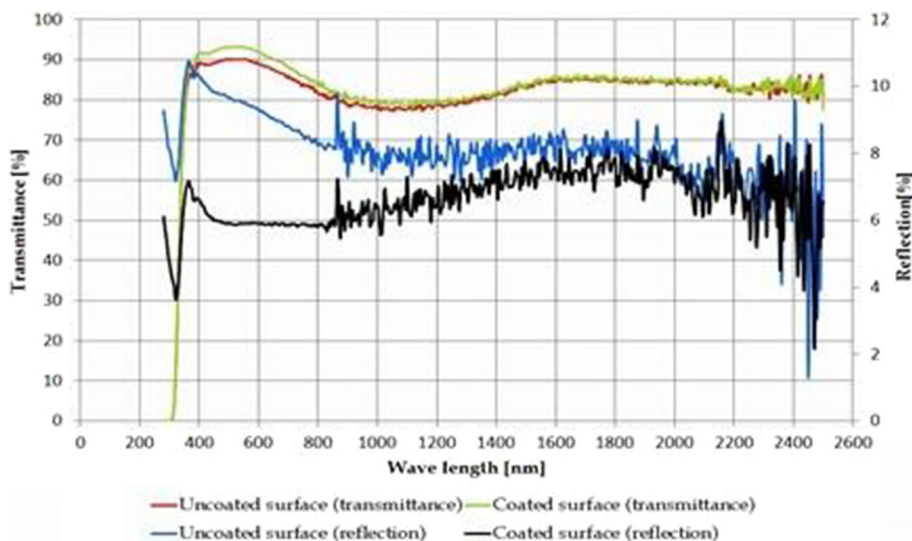


Fig. 9 The spectrometric analysis of Nano-TiO₂ coating on PV panels

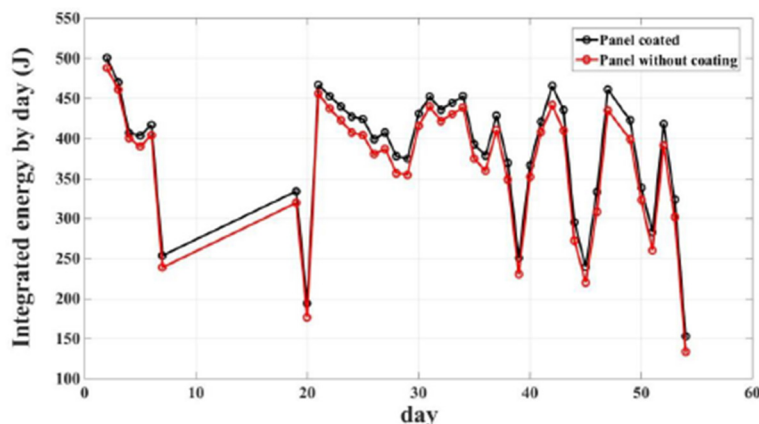


Fig. 10 Integrated energy output of testing solar panels via time

Conclusions

The flow of a liquid film is essential for self-cleaning. To clean a surface, liquid has to transport the impurities and finally run off the surfaces. It is the flowing liquid film that carries away the impurities.

In this study, a 2D dynamic model water film sliding on the inclined non-porous solid surface was established that is based on lubrication theory in association with a precursor film of a wetting liquid on glass.

It is well known that nano-TiO₂ coated glass surfaces display superhydrophilic properties. At the macroscale, by implementing this property into our simulation model, our simulation demonstrates that on superhydrophilic surface, in a very short time, water completely wets the substrate and spreads out into a thin film; on inclined glass surfaces (up to 90°), water droplets/film slide faster on the more hydrophilic surfaces resulting in larger detachment force on particles and better effect on washing away loose particles.

The spectrometric analysis of Nano-TiO₂ coating on glass surface was conducted by our partner in Germany; in the wave length between 400 to 1200 nm, the reflection

on coated surface seems to be 2 ~ 3 % less than that of an uncoated surface; a coated surface shows 2 ~ 3 % more light transmittance than an uncoated surface. This implies Nano-TiO₂ coating itself doesn't show any side effect on the solar cell performance whatsoever. Applying this Nano-TiO₂ coating on a surface of a clean PV/PVT module will potentially increase the efficiency comparing with other coatings which most likely reduce the transmissivity of sunlight.

In Switzerland, four identical solar monocrystalline panels are used for the application of self-cleaning testing under natural weather conditions. Pre-coating, post-coating and extremity tests were conducted, respectively. Our experimental results reveal that the coated panel generated ~3.6 % more energy than that with uncoated panel in a post-coating test. In an extremity test, the coated panel generated ~5.4 % more energy than the one with an uncoated panel in short term test thanks to several major merits of the Nano-TiO₂ coating.

Our entire experiment resulted in a most important conclusion: the coated PV panels distinctively displayed

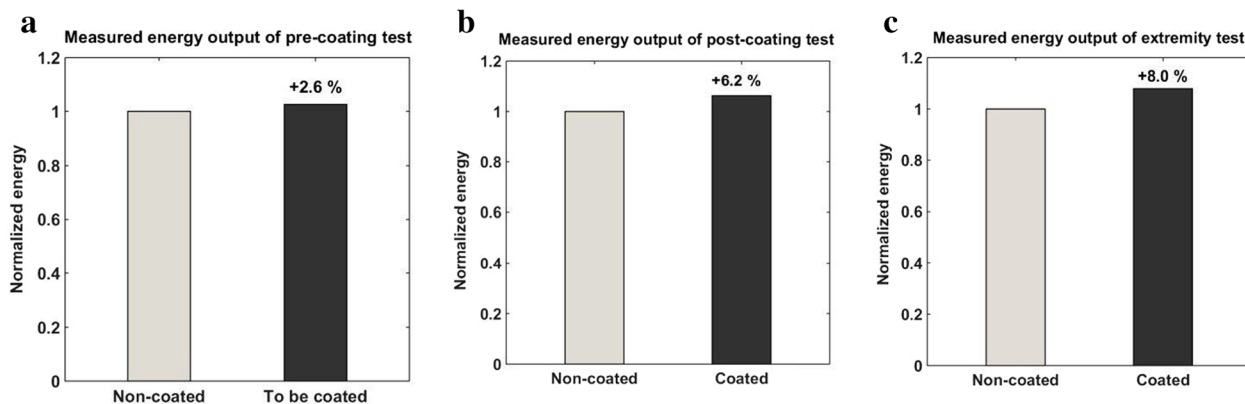


Fig. 11 a Pre-coating test result. b Post-coating test result. c Extremity test result

better “self-cleaning” properties when muddy water was applied. In our cases of extremity test, our PV panel improved performance on an average of over 5 % compared to the non-coated ones. As nano-superhydrophilic coatings are easily applied on glass substrates by common coating techniques, like spraying, dipping, flooding, spinning etc., – considering that large solar power plants cost billions of dollars – this performance boost would save millions of dollars. Many surfaces would be easier to clean and maintain if performed hydrophilic.

This research experiment proved that superhydrophilic surfaces have useful self-cleaning mechanisms, particularly on the glass surfaces of the solar panels. With the weathering that many solar panels undergo, this self-cleaning process may greatly improve the performance and maintenance of solar cells and be a key towards Green Energy in solar cell development. Our research in self-cleaning surfaces can be applied to many other fields as well.

Nomenclature

a , Capillary length (m)

$Ca = \frac{\mu U}{\sigma}$, Capillary number of the runoff equation

C , Prefactor for the power-law

D , Diffusion coefficient ($\text{m}^2 \cdot \text{s}^{-1}$)

$D(\alpha)$, Dimensionless parameter for the runoff equation

δ , film thickness on (m)

g , Gravitational acceleration ($\text{m} \cdot \text{s}^{-2}$)

h' , Adimensional factor for the film thickness (m)

H_0 , Initial droplet or runoff film thickness (m)

h, h^* , Film thickness (m) and dimensionless film thickness

h_{fg} , Latent heat of condensation at the bulk air temperature T_∞ . ($\text{J} \cdot \text{kg}^{-1}$)

I , Current (A)

\mathbf{i} , Unit vector of the x -axis

\mathbf{j} , Unit vector of the y -axis

K, K' , Coefficients of the power law

$Ka = \frac{\gamma}{\mu U}$, Kapitza number

k_b , Thermal conductivity of condensate ($\text{W} \cdot \text{m}^{-1} \cdot \text{K}^{-1}$)

l , radial extension length (m)

L , Adimensional factor for the surface support (m)

L_p , Length of plate (m)

$\nabla = (\partial x, \partial y)$, Nabla operator

R_0 , Drop radius (m)

Re , the Reynolds number

r , Spreading radius (m)

t, t^* , Time (s) and dimensionless time

t_c

T_s , Vapor saturation temperature (297 K)

T_w , Wall temperature (K)

u , Average velocity ($\text{m} \cdot \text{s}^{-1}$)

Velocity component in the x direction ($\text{m} \cdot \text{s}^{-1}$)

u' , Advancing velocity ($\text{m} \cdot \text{s}^{-1}$)

U , Adimensional factor for the velocity ($\text{m} \cdot \text{s}^{-1}$)

Characteristic flow velocity ($\text{m} \cdot \text{s}^{-1}$)

V , Voltage (V)

V , Volume (m^3)

$\mathbf{v} = (u, v)$, Velocity vector

v , Velocity component in the x direction ($\text{m} \cdot \text{s}^{-1}$)

x, x^* , X coordinate (m) and dimensionless x coordinate tangentially to the surface support

x_c , Adimensional factor for x -axis (m)

α , Angle of the inclined plane(rad)

α , Exponent of the power-law

γ , Air-water surface tension ($\text{N} \cdot \text{m}^{-1}$)

μ, μ_b , Dynamic viscosity of liquid ($\text{kg} \cdot \text{m}^{-1} \cdot \text{s}^{-1}$)

ρ , Density of the water ($\text{kg} \cdot \text{m}^{-3}$)

ρ_a , Density of air ($\text{kg} \cdot \text{m}^{-3}$)

θ_D , Dynamic contact angle ($^\circ$)

θ_e, θ_{eq} , Equilibrium contact angle ($^\circ$)

τ , Inertial time scale (s)

Competing interests

The authors declare that they have no significant competing financial, professional or personal interests that might have influenced the performance or presentation of the work described in this manuscript.

Authors' contributions

JH and NB carried out the simulation; JH designed and conducted the experiments. OS and SR supervised the research work. All authors participated in the sequence alignment and drafted the manuscript of paper “CFD simulation and validation of self-cleaning on solar panel surfaces with superhydrophilic coating” for *Future Cities and Environment* Journal, doi:10.1186/s40984-015-0006-7. All authors read and approved the final manuscript.

Acknowledgements

The study is supported by EU HERB project. Special thanks to Mr. Morey Philippe for outdoor experimental setup and data acquisition. The spectrometric analysis of Nano-TiO₂ coating by Mr. Dietrich Schneider at Stuttgart University of Applied Sciences is also acknowledged.

Author details

¹Institute of Thermal Engineering (IGT), University of Applied Sciences of Western Switzerland, Av. des Sports 20, CH-1400 Yverdon-les-Bains, Switzerland. ²Department of Architecture and Built Environment, University of Nottingham, Nottingham, UK.

Received: 14 July 2015 Accepted: 14 July 2015

Published online: 22 August 2015

References

- Ausserre D, Picard AM, Leger L (1986) Existence and role of the precursor film in the spreading of polymer liquids. *Phys Rev Lett* 57:2671–2674
- Bascom WD, Cotto RL, Singletary CR (1964) In Contact Angle, Wettability, and Adhesion. Fowkes FM (ed) ACS, Washington, DC, p 355–379.
- Beaglehole D (1989) Profiles of the precursor of spreading drops of siloxane oil on glass, fused silica, and mica. *J Phys Chem* 93(2):893–899
- Berman A, Drummond C, Israelachvili J (1998) Amontons' law at the molecular level. *Tribol Lett* 4:95–101
- Bertozzi AL, Brenner MP (1997) Linear stability and transient growth in driven contact lines. *Phys Fluids* 9:530
- Biance A-L, Clanet C, Quere D (2004) First steps in the spreading of a liquid droplet. *Phys Rev E* 69:016301
- Bird JC, Mandre S, Stone HA (2008) Short-time dynamic of partial wetting. *Phys Rev Lett* 100:234501
- Blossey R (2003) “Self-cleaning surfaces — virtual realities”. *Nat Mater* 306
- Bonn D, Indekeu J, Meunier J, Rolley E (2009) Reviews of Modern Physics 81(05):739–805

- Carlson A, Do-Quang M, Amberg G (2011) Dissipation in rapid dynamic wetting. *J Fluid Mech* 682:213–240
- Cazabat A-M, Cohen-Stuart MA (1986) Dynamics of wetting: effects of surface roughness. *J Phys Chem* 90:5845
- Chabas A, Lombardo T, Cachier H, Pertuisot MH, Oikonomou K, Falcone R, Verità, M, Geotti-Bianchini, F. (2008) Behaviour of self-cleaning glass in urban atmosphere. *Build Environ* 43(12):2124–2131
- Chen J-D, Wada N (1989) Wetting dynamics near the edge of a spreading drop. *Phys Rev Lett* 62:3050
- Chen L, Auernhammer GK, Bonaccorso E (2011) Short time wetting dynamics on soft surfaces. *Soft Matter* 7:9084–9089
- Dagaonkar M (2012) Effect of fluid flow, solution chemistry and surface morphology of fibrous material on colloid filtration. *J Eng Fibers Fabrics* 7(3):62
- Dagsson-Waldhauserova P, Arnalds O, Olafsson H, Skrabalova L, Sigurdardottir GM, Branis M, Hladil J, Skala R, Navratil T, Chadimova L, von Lowis of Menar S, Thorsteinsson T, Carlsen HK, Jonsdottir I (2014) Physical properties of suspended dust during moist and low wind conditions in Iceland. *Icel Agric Sci* 27(25):25–39
- de Gennes P-G (1985) Wetting: statics and dynamics. *Rev Mod Phys* 57:827
- Diez JA, Kondic L (2002) Computing three-dimensional thin film flows including contact lines. *J Comput Phys* 183:274–306
- Dunnill CWH, Aiken ZA, Pratten J, Wilson M, Morgan DJ, Parkin IP (2009) Enhanced photocatalytic activity under visible light in N-doped TiO₂ thin films produced by APCVD preparations using antibacterial films. *J Photochem Photobiol A* 207(2–3):244–253
- Ehrhard P (1993) Experiments on isothermal and nonisothermal spreading. *J Fluid Mech* 257:463
- Goossens D, Kerschaefer EV (1999) Aeolian dust deposition on photovoltaic solar cells: the effects of wind velocity and airborne dust concentration on cell performance. *Solar Energy* 66:277–289
- Greenspan HP (1978) On the motion of a small viscous droplet that wets a surface. *J Fluid Mech* 84:125
- Hardy WB (1919) The spreading of fluids on glass. *Phil Mag* 38:49–55
- Hardy WB (1936) Collected works. University Press, Cambridge
- Heslot F, Cazabat AM, Levinson P (1989) Dynamics of wetting of tiny drops: ellipsometric study of the late stages of spreading. *Phys Rev Lett* 62:1286–1289
- Heslot F, Cazabat AM, Levinson P (1990) Experiment on wetting on the scale of nanometers: influence of the surface energy. *Phys Rev Lett* 65:599–601
- Hocking LM, Rivers AD (1982) The spreading of a drop by capillary action. *J Fluid Mech* 121:425
- Incropera FP, DeWitt DP (2002) Fundamentals of heat and mass transfer, 5th edn. Wiley, Hoboken, NJ
- Janczuk B, Chibowski E, Staszczuk P (1983) Determination of surface free-energy components of marble. *J Colloid Interface Sci* 96(1):1–6
- Joanny JF, de Gennes PJ (1984) Static structure of wetting films and contact lines. *C R Acad Sci II* 299:279–283
- Katz GB (2008) Effect of Dust on Solar Panels. Available www.gregorybkatz.com/Home/effect-of-dust-on-solar-panels.
- Kavehpour HP, Ovryn B, McKinley GH (2002) Evaporatively-driven marangoni instabilities of volatile liquid films spreading on thermally conductive substrates. *Coll Surf A* 206:409–423
- Kazem HA, Khatib T, Sopian K, Buttinger F, Elmenreich W, Albusaidi AS (2013) Effect of dust deposition on the performance of multi-crystalline photovoltaic modules based on experimental measurements. *Int J Renew Energy Res* 3:4
- Kazmerski L (2011) Photovoltaic: history, technology, markets, manufacturing, applications, and outlook, 84th International Seminar in Brighton, Renewable Energy Policy, Security, Electricity, Sustainable Transport, Water Resources/Management and Environment, Brighton, UK, 3–9.
- Lee A, Moon M-W, Lim H, Kim W-D, Kim H-Y. (2012) Water harvest via dewing. *Langmuir* 28(27):10183–10191.
- Levinson P, Cazabat A-M, Cohen-Stuart MA, Heslot F, Nicolet S (1988) The spreading of macroscopic droplets. *Rev Phys Appl* 23:1009
- Lopez J, Miller CA, Ruckenstein E (1976) Spreading kinetics of liquid drops on solids. *J Colloid Interface Sci* 53:460–461
- Marmur A, Lelah MD (1980) The dependence of drop spreading on the size of the solid surface. *J Colloid Interf Sci* 78(262):265
- Noguchi H, Hiroshi M, Tominaga T, Gong JP, Osada Y, Uosaki K (2008) Interfacial water structure at polymer gel/quartz interfaces investigated by sum frequency generation spectroscopy. *Phys Chem Chem Phys* 10:4987–4993, PubMed:18688544
- Ohtsu N, Masahashi N, Mizukoshi Y, Wagatsuma K (2009) Hydrocarbon decomposition on a hydrophilic TiO₂ surface by UV irradiation: spectral and quantitative analysis using in situ XPS technique. *Langmuir* 25(19):11586–11591
- Oron A, Davis SH, Bankoff SG (1997) Long-scale evolution of thin liquid films. *Rev Mod Phys* 69(3):931
- Perevertaev VD, Metsik MS, Golub LM (1979) Dependence of the heat of adsorption of water-molecules on the activity of the surface of muscovite crystals. *Colloid J USSR* 41(1):124–126, *Phys.* 12:1473 – 1484, 1979
- Rafai S, Sarker D, Bergeron V, Meunier J, Bonn D (2002) Superspreading: aqueous surfactant drops spreading on hydrophobic surfaces. *Langmuir* 18(26):10486–10488
- Raviv U, Perkin S, Laurat P, Klein J (2004) Fluidity of water confined down to subnanometer films. *Langmuir* 20:5322–5332
- Razouk RI, Salem AS (1948) The adsorption of water vapor on glass surfaces. *J Phys Chem* 52(7):1208–1227
- Rhykerd CL, Cushman JH, Low PF (1991) Application of multiple-angle-of-incidence ellipsometry to the study of thin fluid films adsorbed on surfaces. *Langmuir* 7(10):2219–2229
- Ruths M, Israelachvili JN (2011) Chapter 13, surface forces and nanorheology of molecularly thin films. In: Bhushan B (ed) *Nanotribology and nanomechanics*. Springer-Verlag, Berlin Heidelberg
- Sah A (2014) Precursor film: a key driver to determine wetting behavior in the vicinity of surface heterogeneity. *Soft Matter* 10:3890–3896
- Salim A, Huraib F, Eugenio N (1988) PV power-study of system options and optimization. In: *Proceedings of the 8th European PV Solar Energy Conference*. Florence, Italy
- Sayigh A (2009) Worldwide progress in renewable energy. *Renewable Energy*. Sciverse Science Direct. 20 November 2009:1-5.
- Sayigh A, Al-Jandal S, Ahmed H (1985) Dust effect on solar flat surfaces devices in Kuwait. In: *Proceedings of the workshop on the physics of Non-conventional energy sources and materials science for energy*. Trieste, Italy, pp 353–367
- Sharma BK (1994) Air pollution, ISBN: 81-8283-014-1.
- Smith SH (1969) On initial value problems for the flow in a thin sheet of viscous liquid. *J Appl Math Phys (ZAMP)*, 20, 556–560
- Smith JD, Cappa CD, Wilson KR, Messer BM, Cohen RC, Saykally RJ (2004) Energetics of hydrogen bond network rearrangements in liquid water. *Science* 306:851–853 [PubMed: 15514152]
- Stapelbroek BBJ, Jansen HP, Kooij ES, Snoeijer JH, Eddi A (2014) Universal spreading of water drops on complex surfaces. *Soft Matter* 10:2641
- Staszczuk P (1985) Application of the chromatographic step profile method for determination of water film pressure and surface freeenergy of quartz. *Chromatographia* 20(12):724–728
- Tanner LH (1979) The spreading of silicone oil drops on horizontal surfaces. *J Phys D Appl Phys* 12:1473–1484
- Tian C, Ji N, Waychunas GA, Shen YR (2008) Interfacial structures of acidic and basic aqueous solutions. *J Am Chem Soc* 130:13033–13039, PubMed: 18774819
- Troian SM, Herbolzheimer E, Safran SA, Joanny JF (1989) Fingering instabilities of driven spreading films". *Europhys Lett* 10:25
- Ueno I, Watanabe T (2005) Dynamic behavior of precursor liquid film in front of moving droplet on solid, 16th International Symposium on Transport Phenomena, ISTEP-16, Prague.
- Valignat MP, Oshanian G, Villette S, Cazabat A-M, Moreau M (1998) Molecular weight dependence of spreading rates of ultrathin polymeric films. *Phys Rev Lett* 80:5377–5380
- Villette S, Valignat MP, Cazabat AM, Jullien L, Tiberg F (1996) Wetting on the molecular scale and the role of water. A case study of wetting of hydrophilic silica surfaces. *Langmuir* 12:825–830
- Voinov OV (1976) Hydrodynamics of wetting. *Fluid Dynamics* 11:714–721
- Vou'e M, Valignat MP, Oshanian G, Cazabat A-M (1999) Dissipation processes at the mesoscopic and molecular scale. The case of polymer films. *Langmuir* 15:1522–1527
- Wack KO (1980) "Cleaning system for solar energy collectors", *Physics Abstract Science*
- Wakim F (1981) Introduction of PV power generation to Kuwait. Kuwait Institute for Scientific Researchers, Kuwait City
- Wang XD (2003) Contact angle hysteresis and dynamic wetting behavior on rough solid surfaces, Ph.D. Thesis. Tsinghua University, China

- Winkels KG, Weijs JH, Eddi A, Snoeijer JH (2012) Initial spreading of low-viscosity drops on partially wetting surfaces. *Phys Rev E* 85(5):055301
- Yeo L (2008) Wetting and Spreading, *Encyclopedia of Microfluidics and Nanofluidics*, pp 2186–2196
- Yoo H, Paranj R, Pollack GH (2011) Impact of hydrophilic surfaces on interfacial water dynamics probed with NMR spectroscopy. *J Phys Chem Lett* 2(6):532–536
- Yuan Q, Zhao Y-P (2010) Precursor film in DynamicWetting, electrowetting, and electro-elasto-capillarity. *Phys Rev Lett*, Prl 104:246101
- Zisman WA (1965) Improving the performance of reinforced plastics. *Ind Eng Chem* 57:26–34
- Zoetewij ML, van der Donck JCJ, Versluis R (2009) Particle removal in linear shear flow: model prediction and experimental validation. *J Adh Sci Technol* 23(6):899–911

Submit your manuscript to a SpringerOpen[®] journal and benefit from:

- ▶ Convenient online submission
- ▶ Rigorous peer review
- ▶ Immediate publication on acceptance
- ▶ Open access: articles freely available online
- ▶ High visibility within the field
- ▶ Retaining the copyright to your article

Submit your next manuscript at ▶ springeropen.com
